

# Proton's Electromagnetic Form Factors from a Non-Power Confinement Potential

M. Kirchbach\*

*Instituto de Física, Universidad Autónoma de San Luis Potosí,  
Av. Manuel Nava 6, Zona Universitaria, San Luis Potosí, S.L.P. 78290, México*

C.B.Compean

*Facultad de Ciencias, Universidad Autónoma de San Luis Potosí Lateral  
Av. Salvador Nava s/n, San Luis Potosí, S.L.P. 78290, México*

The electric-charge, and magnetic-dipole form factors of the proton are calculated from an underlying constituent quark picture of hadron structure based on a potential shaped after a cotangent function, which has the properties of being both conformally symmetric and color confining, finding adequate reproduction of a variety of related data.

PACS numbers: 12.38.Am, 12.39.Pn, 13.40.Em

Keywords: General properties of QCD, Potential models, Electric and magnetic moments

## Contents

<b>I. Introduction</b>	1
<b>II. Gauging on <math>S^3</math> the Dirac equation with the cotangent potential and the road of the super-symmetric quantum mechanics to its solutions</b>	3
A. General form of the “quasi-radial” Dirac spinors	6
B. The “quasi-radial” Dirac spinor for the ground state of the proton	7
C. Comparison of the “quasi-radial” Dirac spinors to the two-component wave functions in the Light-Front Holographic QCD	8
<b>III. The proton electric-charge and magnetic-dipole form factors</b>	9
<b>IV. Summary and conclusions</b>	15
<b>References</b>	16

## I. INTRODUCTION

Constituent quark model descriptions of hadron properties, such as excitation spectra, decay modes, or electromagnetic form-factors, employ quantum few-body problems techniques based on effective potentials [1] supposed to capture to some extent the essentials of the fundamental confining strong interaction. The potentials of widest spread in the literature are shaped after power-functions of the relative distances between the quarks, and among them one encounters for example (i) the infinite-power square-well potential,  $V_{SW}(r) = 1/r^\infty = 0$ ,  $0 \leq r \leq r_0$ , and  $V(r) = r^\infty = \infty$  for,  $-\infty < r < 0$  and  $r > r_0$ , (ii) the harmonic oscillator,  $V_{HO}(r) = \omega^2 r^2/2$ , (iii) the Cornell potential,  $V_C(r) = -\alpha/r + \beta r$ , etc. Such models usually require a significant number of free parameters to produce wave functions of the quark systems capable to account for the specific of a variety of data compiled in [2]. One of the reasons for this circumstance can be related to the mismatch between the symmetry properties of the power-potentials and the symmetries of the fundamental strong interaction like the conformal symmetry, which manifests itself among others by the walking of the strong coupling  $\alpha_s$  to a fixed value in the infrared regime of QCD [3] and the notable hydrogen-like degeneracies appearing in the mass distributions of the unflavored mesons, a phenomenon addressed for example in [4], [5], [6]. In order to improve this aspect of the quark models, it naturally comes to ones mind to explore more complicated potential functions. The observation that the infinite square well has same spectrum as the  $[2 \csc^2(\pi r/r_0) - 1]$  potential, referred to in [7] as the “super-symmetric partner” to  $V_{SW}(r/r_0)$ , seems

---

\*Electronic address: mariana@ifisica.uaslp.mx

to point toward the exactly solvable trigonometric potentials known from the super-symmetric quantum mechanics (SUSY-QM), as possible upgrades to the power-potentials. Indeed, several of the finite power-potential series in use can be viewed as first terms in the infinite series expansions of properly designed trigonometric functions. Specifically, the (here dimensionless) inverse square distance term,  $R^2/r^2$  where  $R$  is a matching length parameter, approximates  $\csc^2(r/R)$  at small  $(r/R)$  values. The linear plus harmonic oscillator potential can be viewed as an approximation to the trigonometric Scarf potential,

$$\begin{aligned} V_{tSc} \left( \frac{r}{R} \right) &= [b^2 + a(a+1)] \sec^2 \left( \frac{r}{R} \right) - b(2a+1) \sec \left( \frac{r}{R} \right) \tan \left( \frac{r}{R} \right) \\ &\approx -b(2a+1) \frac{r}{R} + [b^2 + a(a+1)] \left( \frac{r}{R} \right)^2, \end{aligned} \quad (1.1)$$

by the first terms of its series expansion, while the Cornell potential could be viewed as a truncation of the series expansion of the cotangent function according to,

$$-b \cot \left( \frac{r}{R} \right) \approx -b \frac{R}{r} + \frac{b}{3} \frac{r}{R}. \quad (1.2)$$

The principal advantage of trigonometric- over finite power potentials lies not that much in the exact solubility of the former, but rather in their symmetry properties, which show up in certain appropriately chosen variables. For example, while the centrifugal barrier,  $\ell(\ell+1)/r^2$ , and the Cornell potential are only rotationally symmetric, their trigonometric extensions towards  $\ell(\ell+1) \csc^2(r/R)$  and  $-\cot(r/R)$  have the higher  $O(4)$  symmetry, just as would be required by the conformal symmetry at the level of the excitations. This is visible from the fact that the stationary Schrödinger wave equation, describing (upon separation of center-of mass and relative,  $r/R$ , coordinates) the one-dimensional radial part

$$\left[ -\frac{\hbar^2 c^2}{R^2} \frac{d^2}{d\chi^2} + \frac{\hbar^2 c^2}{R^2} \frac{\ell(\ell+1)}{\sin^2 \chi} - 2 \frac{\hbar^2 c^2 b^2}{R^2} \cot \chi \right] U_{n\ell}(\chi) = \mathcal{E}^2 U_{n\ell}(\chi), \quad \chi = \frac{r}{R} \in [0, \pi], \quad (1.3)$$

of a two-body wave function, with  $n$  being the node-number, and  $\ell$  the relative angular momentum value, can be transformed through the change

$$U_{n\ell}(\chi) Y_\ell^m(\theta, \varphi) = \frac{\Psi_{n\ell}(\chi)}{\sin \chi} Y_\ell^m(\theta, \varphi) = \Psi_{n\ell}^{tot}(\chi, \theta, \varphi), \quad (1.4)$$

to quantum motion on the three dimensional hypersphere,  $S^3$ , according to

$$\begin{aligned} \frac{\hbar^2 c^2}{R^2} [\mathcal{K}^2(\chi, \theta, \varphi) - 2b^2 \cot \chi] \Psi_{n\ell}^{tot}(\chi, \theta, \varphi) &= \left( \mathcal{E}^2 - \frac{\hbar^2 c^2}{R^2} \right) \Psi_{n\ell}^{tot}(\chi, \theta, \varphi), \\ \mathcal{E}^2 = \frac{\hbar^2 c^2}{R^2} (K+1)^2 - \frac{\hbar^2 c^2}{R^2} \frac{b^2}{(K+1)^2}, \quad K = n + \ell. \end{aligned} \quad (1.5)$$

Here,  $\chi$  and  $R$  take in their turn the rôle of the second polar angle, and hyper-spherical radius,  $\theta$  and  $\varphi$  are the polar and azimuthal angles in ordinary three space,  $\mathcal{K}^2(\chi, \theta, \varphi)$  stands for the squared four-dimensional angular momentum operator, and  $K$  for its value. In other words,  $\mathcal{K}^2(\chi, \theta, \varphi)$  represents the angular part of the Laplacian  $\Delta_4(R, \chi, \theta, \varphi)$  of the four dimensional Euclidean space in global coordinates according to,

$$\Delta_4(R, \chi, \theta, \varphi) = \frac{1}{R^3} \frac{\partial}{\partial R} R^3 \frac{\partial}{\partial R} - \frac{1}{R^2} \mathcal{K}^2(\chi, \theta, \varphi), \quad (1.6)$$

meaning that at a constant hyper-radius,  $R = \text{const}$ , one finds it expressed as,

$$\frac{1}{R^2} \mathcal{K}^2(\chi, \theta, \varphi) = -\Delta_4(R, \chi, \theta, \varphi)|_{R=\text{const}} = \frac{1}{R^2 \sin^2 \chi} \frac{\partial}{\partial \chi} \sin^2 \chi \frac{\partial}{\partial \chi} + \frac{L^2(\theta, \varphi)}{R^2 \sin^2 \chi}, \quad (1.7)$$

where  $L^2(\theta, \varphi)$  is the ordinary operator of the squared angular momentum whose eigenfunctions are the spherical harmonics,  $Y_\ell^m(\theta, \varphi)$ . In this way, the  $\csc^2 \chi$  term acquires meaning of the centrifugal term on  $S^3$ . Now, the product of  $U_{n\ell}(\chi)$  by the standard spherical harmonic,  $Y_\ell^m(\theta, \varphi)$  in (1.4) represents the complete three dimensional

“curved” wave function,  $\Psi_{n\ell}^{tot}(\chi, \theta, \varphi)$ .

There is one particularly remarkable aspect of the equations (1.6)-(1.7) which is that under the variable changes,

$$R = e^\tau, \quad R \sin \chi = r, \quad (1.8)$$

with  $r$  being the radial variable on the equatorial disc of  $S^3$ , a plane three dimensional Euclidean space, the Laplacian  $\Delta_4(R, \chi, \theta, \varphi)$  is transformed to

$$\Delta_4(R, \chi, \theta, \varphi) \longrightarrow e^{-2\tau} \left[ \frac{\partial^2}{\partial \tau^2} - \frac{1}{r^2} \frac{\partial}{\partial r} r^2 \frac{\partial}{\partial r} - \frac{1}{r^2} \frac{L_2^2(\varphi)}{\sin^2 \theta} \right], \quad (1.9)$$

in the approximation  $R \sin \chi \approx R\chi$ . Here,  $L_2^2(\varphi)$  is the operator of the squared angular momentum on the plane (for details see [8]). The latter equation is the Laplacian of an “effective” Minkowskian space-time with the place of the ordinary time variable being occupied by the so called “conformal time”  $\tau$ , the logarithm of the hyper radius. In this way, a Minkowskian metric can be associated with the closed space. This is an essential point to which we shall come back in due place below.

Back to (1.5), all states with  $n + \ell = K$  and  $K$  integer (the value of the four-dimensional angular momentum) have same energy. Along these lines the excitations of the unflavored mesons over the ground state energy (treated as a parameter) could be satisfactorily adjusted in [9], [10] up to about 2500 MeV by means of the constants  $b$ , and  $R$ . Moreover, there we also presented along the lines of refs. [11], [12] rigorous mathematical considerations relating the cotangent function to a cusped Wilson loop on  $S^3$ , which allowed in due course to reveal its color confining nature. Namely, we showed that the magnitude of the cotangent function can be expressed in terms of the strong coupling  $\alpha_s$  and the number of colors,  $N_c$ , as

$$2b = \alpha_s N_c. \quad (1.10)$$

In effect, in the coordinates of (1.7), the conformal and color confining properties of the cotangent function have been made manifest.

We then inserted the parametrization given by (1.10) in (1.5) to perform our data analyzes, and interpreted  $\alpha_s$  as an effective QCD inspired potential parameter. Upon extracting the  $\alpha_s$  values from the mass distribution of 71 measured mesons, organized into four Regge-trajectory families, we found that they quite conveniently matched data for the mass ranges of the ground state mesons under consideration. Encouraged by the satisfactory meson data analyzes by the potential in (1.3), we here aim to extend the method briefly reviewed above to fermion description with the task to test the proton’s electromagnetic form factors.

The article is structured as follows. The next section is dedicated to the Dirac equation gauged by the cotangent potential. There, we consider this equation in a specific approximation which then allows for exact solubility by the aids of techniques established by the super-symmetric quantum mechanics (SUSY-QM), and construct the Dirac spinors. In due course we encounter that the upper and lower Dirac spinor components satisfy a pair of coupled one-dimensional Schrödinger equations which parallel in the infrared the two coupled one-dimensional equations of the Light-Front Holographic QCD [13], [14]. In Section 3 we employ the Dirac spinors obtained in this way in the calculations of the proton’s and neutron’s electric-charge, and magnetic dipole form-factors, as well as in the ratio of the proton’s form-factors, finding good agreement with data. The text closes with a concise Summary and Conclusion Section.

## II. GAUGING ON $S^3$ THE DIRAC EQUATION WITH THE COTANGENT POTENTIAL AND THE ROAD OF THE SUPER-SYMMETRIC QUANTUM MECHANICS TO ITS SOLUTIONS

In this section we formulate the Dirac equation gauged by the cotangent potential and construct its solutions with the aim to employ them in the subsequent section in the calculation of the proton’s electromagnetic form factors. Among the many coordinates in which a Dirac equation with a cotangent gauge potential can be formulated we choose the polar coordinates corresponding to the three-dimensional space of a constant curvature given by the hypersphere  $S^3$ , because this specific chart provides a stage suited for modelling the confinement phenomenon in so far as no free charges can exist on such spaces, a textbook knowledge [15]. The minimal charge configurations allowed to exist on such a geometry are color dipoles, i.e. color neutral states, just as required by confinement, and the potential produced by a color dipole is just a cotangent function [9],[10], a reason for which we shall frequently refer to this potential as “color confining dipole (CCD)” interaction. Noticing furthermore that instantaneous

potentials describe virtual processes happening outside of the causal light cone, allows to interpret the dynamics in (1.5) as quantum motion on a hypersphere located outside the light cone. Such a geometry can appear as (the only) closed space-like geodesic of a four dimensional hyperboloid of one sheet, a so called  $dS_4$  space, known to foliate the space-like region within the framework of the so called “de Sitter special relativity” [16], which hypothesizes the virtual region of the Minkowskian space to have one more space-like dimension. More details can be found in [9]. Below we shall incorporate the cotangent color confining dipole function as a gauge interaction in the Dirac equation. Using Riemannian spaces to simulate gauge interactions at distinct energy scales (regimes), is in principle legitimate according to [17], because of the dichotomy between Riemann’s curvature and field-strength tensors, though non-Abelian theories require special care as in this case the Gauss law, among others, becomes more involved [18]. It needs furthermore to be admitted that so far only for  $SU(2)$  non-Abelian gauge group the identification of gauge spaces by a 3D Riemannian manifolds (as is the  $S^3$  geodesic of the  $dS_4$  Riemannian space from above) could be fully justified in the literature, while the  $SU(3)_c$  case of QCD is lots more complicated [19] and still under investigation. In view of this, we here limit ourselves to consider the cotangent function from above as a Riemannian space inspired phenomenological QCD interaction in the infrared.

The free Dirac equation on  $S^3$  is well elaborated in the literature and is given by

$$\begin{aligned} \left[ i\hbar c \tilde{\nabla}_\mu \tilde{\gamma}^\mu(x) - mc^2 \right] \psi(x) &= 0, \\ \{ \tilde{\gamma}^\mu(x), \tilde{\gamma}^\nu(x) \} &= 2g^{\mu\nu}(x), \quad x = (x_0, x_1, x_2, x_3), \end{aligned} \quad (2.1)$$

where  $\psi(x)$  is a four-component spinor,  $g^{\mu\nu}(x)$  is the  $S^3$  metric tensor,  $\tilde{\nabla}_\mu(x)$  is a *spin covariant* derivative on  $S^3$ , while  $\tilde{\gamma}^\mu(x)$  are the Dirac matrices on the manifold under consideration (for details see [20], among others). It is common to re-parametrize the hypersphere, defined as  $x_0^2 + x_1^2 + x_2^2 + x_3^2 = R^2$ , in terms of global coordinates according to,  $x_0 = R \cos \chi$ ,  $x_3 = R \sin \chi \cos \theta$ ,  $x_1 = R \sin \chi \sin \theta \cos \varphi$ , and  $x_2 = R \sin \chi \sin \theta \sin \varphi$ , with  $\chi, \theta \in [0, \pi]$ , and  $\varphi \in [0, 2\pi]$ . The algebra of (2.1) has been worked out in great detail in [20], [21] in connection with the particular case of a  $\psi(x)$  coupled to a cotangent potential produced by an electromagnetic source. There the authors show that upon variable separation,  $\psi(x) \rightarrow \Psi(R, \chi, \theta, \varphi) = \Psi_{j\ell}(R, \chi) Y_L^M(\theta, \varphi)$ , with  $Y_L^M(\theta, \varphi)$  being the standard spherical harmonics, one encounters in the variable  $\chi$ , frequently termed to as “quasi-radial” in the literature, the following system of two linear coupled equations ,

$$\begin{aligned} \frac{\hbar c}{R} \left( \frac{d}{d\chi} + \frac{(-1)^{j+\ell+\frac{1}{2}} (j + \frac{1}{2})}{\sin \chi} \right) G_{j\ell}(\chi) &= \left( E_{j\ell} + mc^2 + \frac{\hbar c}{R} \alpha Z \cot \chi \right) F_{j\ell}(\chi), \\ \frac{\hbar c}{R} \left( -\frac{d}{d\chi} + \frac{(-1)^{j+\ell+\frac{1}{2}} (j + \frac{1}{2})}{\sin \chi} \right) F_{j\ell}(\chi) &= \left( mc^2 - E_{j\ell} + \frac{\hbar c}{R} \alpha Z \cot \chi \right) G_{j\ell}(\chi), \\ j &= \ell \pm \frac{1}{2}, \quad \ell \geq 0, \end{aligned} \quad (2.2)$$

where  $\alpha = e^2/(4\pi\hbar c)$  is the fundamental electromagnetic constant, and  $Z$  is the number of charges in the potential source. Furthermore,  $G_{j\ell}(\chi)$ , and  $F_{j\ell}(\chi)$ , relate to the respective upper and lower components of the “quasi-radial” Dirac spinor,  $\Psi_{j\ell}(R, \chi)$ , according to

$$\Psi_{j\ell}(R, \chi) = \begin{pmatrix} \frac{iG_{j\ell}(\chi)}{R \sin \chi} \\ \frac{F_{j\ell}(\chi)}{R \sin \chi} \end{pmatrix}, \quad \text{with} \quad \int_0^\pi (G_{j\ell}^2(\chi) + F_{j\ell}^2(\chi)) d\chi = 1. \quad (2.3)$$

Our case relates to (2.2) through the replacements,

$$-\frac{\hbar c}{R} \alpha Z \cot \chi \Rightarrow -\frac{\hbar c}{R} \alpha_s N_c \cot \lambda\chi, \quad \alpha_s = \frac{g_s^2}{4\pi\hbar c}, \quad \lambda\chi \in [0, \pi]. \quad (2.4)$$

The  $mc^2$  parameter entering the eqs. (2.2) is the reduced mass of the constituents of the two-body spin-1/2 composite system, considered upon the reduction of the two-body to one-body problem to move in the gauge potential. In the flat space case of the H atom this degree of freedom is a spin-1/2 electron of a single charge. However, on  $S^3$ , where no single charges can be defined, a spin-1/2 degree of freedom has to be a charge dipole, such as a spin-1/2 (quark)-(anti-symmetric scalar diquark) configuration of the proton. The potential source can be then thought of as an effective scalar gluon-anti-gluon background. In the following, the influence of the former dipole on the latter. i.e. the tensor force between the two dipoles, will be neglected. Within this picture,  $mc^2$  denotes the reduced mass

of the quarkish and gluonic color dipoles. The introduction of the  $\lambda$  constant in the “quasi-radial” variable will become clear in due course.

The equations in (2.2) are claimed in [22] to be exactly solvable in terms of Heun’s polynomials. We here instead adopt the approximation of the kinetic term used in [20],

$$\frac{\hbar c}{R \sin \lambda \chi} \approx \frac{\hbar c}{R} \cot \lambda \chi + \mathcal{O}\left(\frac{1}{R^2}\right), \quad (2.5)$$

amounting to the following, also exactly solvable, matrix equation,

$$\begin{aligned} \frac{\hbar c}{R} \begin{pmatrix} \frac{dG_{j\ell}(\chi)}{d\chi} & 0 \\ 0 & \frac{dF_{j\ell}(\chi)}{d\chi} \end{pmatrix} + \frac{\hbar c}{R} \cot \lambda \chi \begin{pmatrix} k & -\gamma \\ \gamma & -k \end{pmatrix} \begin{pmatrix} G_{j\ell}(\chi) \\ F_{j\ell}(\chi) \end{pmatrix} \\ = \begin{pmatrix} 0 & E_{j\ell} + mc^2 \\ mc^2 - E_{j\ell} & 0 \end{pmatrix} \begin{pmatrix} G_{j\ell}(\chi) \\ F_{j\ell}(\chi) \end{pmatrix}. \end{aligned} \quad (2.6)$$

The following notions have been introduced

$$k = (-1)^{\ell+j+\frac{1}{2}} \left(j + \frac{1}{2}\right), \quad \gamma = \alpha_s N_c. \quad (2.7)$$

From a purely technical point of view, the approximation to the Dirac equation on  $S^3$  by (2.6) allows for a treatment in exact parallel to the flat-space Dirac equation with the Coulomb potential, and along the line presented, for example, in [23]. For this purpose the equation (2.6) has to be similarity transformed by the following matrix,

$$D = \begin{pmatrix} k+s & -\gamma \\ -\gamma & k+s \end{pmatrix}, \quad s = \sqrt{k^2 - \gamma^2} = \sqrt{\left(j + \frac{1}{2}\right)^2 - \alpha_s^2 N_c^2}, \quad (2.8)$$

$$D^{-1} = \frac{1}{2s(s+k)} \begin{pmatrix} k+s & \gamma \\ \gamma & k+s \end{pmatrix}, \quad D \begin{pmatrix} k & -\gamma \\ \gamma & -k \end{pmatrix} D^{-1} = \begin{pmatrix} s & 0 \\ 0 & -s \end{pmatrix}, \quad (2.9)$$

with the result being the following two coupled linear equations

$$\left[\frac{\hbar c}{R} \frac{d}{d\chi} + W(\chi)\right] \tilde{G}_{n'\ell'}^j(\chi) = \left(mc^2 + \frac{k}{s} E_{j\ell}\right) \tilde{F}_{n\ell}^j(\chi), \quad (2.10)$$

$$\left[-\frac{\hbar c}{R} \frac{d}{d\chi} + W(\chi)\right] \tilde{F}_{n\ell}^j(\chi) = \left(mc^2 - \frac{k}{s} E_{j\ell}\right) \tilde{G}_{n'\ell'}^j(\chi), \quad (2.11)$$

$$n' + \ell' = n + \ell, \quad W(\chi) = -\frac{\hbar c}{R} s \cot \lambda \chi - \frac{\gamma}{s} E_{j\ell}, \quad (2.12)$$

with

$$\tilde{\Psi}_{j\ell}(R, \chi) = \begin{pmatrix} \tilde{G}_{n'\ell'}^j(\chi) \\ \tilde{F}_{n\ell}^j(\chi) \end{pmatrix} = \begin{pmatrix} k+s & -\gamma \\ -\gamma & k+s \end{pmatrix} \begin{pmatrix} G_{j\ell}(\chi) \\ F_{j\ell}(\chi) \end{pmatrix}, \quad (2.13)$$

where we introduced the intermediate auxiliary spinor  $\tilde{\Psi}_{j\ell}(R, \chi)$ . The inclusion of the node number  $n$  into the labeling of the components  $\tilde{G}$ , and  $\tilde{F}$ , of the auxiliary spinors will become clear in due course, and is advantageous within the SUSY-QM framework [7], on which [23] is based. There, the left hand sides of the equations (2.10) and (2.11) are defined by the so called up- and down ladder operators, respectively, denoted by

$$A^+(\chi) = \frac{\hbar c}{R} \frac{d}{d\chi} + W(\chi), \quad (2.14)$$

$$A^-(\chi) = -\frac{\hbar c}{R} \frac{d}{d\chi} + W(\chi), \quad (2.15)$$

with the  $W(\chi)$  function being termed to as a “super-potential”. As it will become clear below, one of the tasks of the ladder operators is to shift the node number by one unit, so that  $n' = n - 1$ . By means of them, the equations

(2.10)-(2.11) are cast in the elegant form of

$$A^+(\chi)\tilde{G}_{n'\ell}^j(\chi) = E_{j\ell}^{(1)}\tilde{F}_{n\ell}^j(\chi), \quad n' = n - 1, \quad \ell' = \ell + 1, \quad (2.16)$$

$$A^-(\chi)\tilde{F}_{n\ell}^j(\chi) = E_{j\ell}^{(2)}\tilde{G}_{n'\ell'}^j(\chi), \quad (2.17)$$

$$\begin{aligned} E_{j\ell}^{(1)} &= mc^2 + \frac{k}{s}E_{j\ell}, & E_{j\ell}^{(2)} &= mc^2 - \frac{k}{s}E_{j\ell}, \\ E_{j\ell}^{(1)} &\neq E_{j\ell}^{(2)} & \text{for } mc^2 &\neq 0. \end{aligned} \quad (2.18)$$

It is straightforward to check that the two coupled linear equations in (2.10)-(2.11) are equivalent to the following two decoupled quadratic equations

$$\left(-\frac{\hbar^2 c^2}{R^2} \frac{d^2}{d\chi^2} + V_1(\chi)\right)\tilde{G}_{n'\ell'}^j(\chi) = \left(\frac{k^2 E_{j\ell}^2}{s^2} - m^2 c^4\right)\tilde{G}_{n'\ell'}^j(\chi), \quad (2.19)$$

$$\left(-\frac{\hbar^2 c^2}{R^2} \frac{d^2}{d\chi^2} + V_2(\chi)\right)\tilde{F}_{n\ell}^j(\chi) = \left(\frac{k^2 E_{j\ell}^2}{s^2} - m^2 c^4\right)\tilde{F}_{n\ell}^j(\chi), \quad (2.20)$$

with the potentials  $V_1(\chi)$  and  $V_2(\chi)$  being given as,

$$\begin{aligned} V_1(\chi) &= W(\chi)^2 - \frac{\hbar c}{R}W'(\chi) = \frac{\hbar^2 c^2}{R^2} \frac{(s+1)(s+1-\lambda)}{\sin^2 \lambda\chi} - 2\frac{\hbar c}{R}\gamma E_{j\ell} \cot \lambda\chi \\ &\quad - \frac{\hbar^2 c^2}{R^2} s^2 + \frac{\gamma^2}{s^2} E_{j\ell}^2, \end{aligned} \quad (2.21)$$

$$\begin{aligned} V_2(\chi) &= W(\chi)^2 + \frac{\hbar c}{R}W'(\chi) = \frac{\hbar^2 c^2}{R^2} \frac{s(s-\lambda)}{\sin^2 \lambda\chi} - 2\frac{\hbar c}{R}\gamma E_{j\ell} \cot \lambda\chi \\ &\quad - \frac{\hbar^2 c^2}{R^2} s^2 + \frac{\gamma^2}{s^2} E_{j\ell}^2. \end{aligned} \quad (2.22)$$

The dependence of the magnitude of the cotangent potential on the energy,  $E_{j\ell}$ , represents the genuine signature for the origin of the SUSY-QM equations from a Dirac equation. Both the  $V_1(\chi)$ , and  $V_2(\chi)$  interactions are shaped after a function known in SUSY-QM under the name of the trigonometric Rosen-Morse potential, and the two, in being in addition isospectral, are termed to as ‘‘partner potentials’’. In this particular case the isospectrality is ensured by obtaining  $V_1(\chi)$  from  $V_2(\chi)$  by the replacements,  $s \rightarrow s + 1$ , and  $n' = (n - 1)$ , everywhere besides in the constants, thus keeping  $(s + n) = (s + 1 + n')$  unaltered (see Fig. 1 for a graphical interpretation).

In the following, we shall set  $\lambda = -1$ , in which case  $s(s - \lambda) \csc^2 \lambda\chi \rightarrow s(s + 1) \csc^2 \chi$  for  $V_2(\chi)$ , while in  $V_1(\chi)$  this term becomes,  $(s + 1)(s + 1 - \lambda) \csc^2 \lambda\chi \rightarrow (s + 1)(s + 2) \csc^2 \chi$ , a choice which, contrary to  $\lambda = 1$ , will lead to everywhere finite probability densities. In this sense, the rescaling of the ‘‘quasi-radial’’ variable by the  $\lambda$  parameter introduced here by us can be viewed as a regularization scheme, different from the one used in the case of the H Atom to avoid the singularity of its Dirac ground state spinor [24].

### A. General form of the ‘‘quasi-radial’’ Dirac spinors

The (unnormalized) wave functions solving (2.20)-(2.22) are known and available in the literature. In the particular form constructed by [25], and reviewed in [26], they are given by

$$\tilde{F}_{n\ell}^j(\chi) = R^{-\beta_n} \sin^{-\beta_n} \chi e^{-\frac{\alpha_n \chi}{2}} R_n^{(\alpha_n, \beta_n)}(\cot \chi), \quad (2.23)$$

$$\beta_n = -(n + s + 1), \quad \alpha_n = \frac{2\gamma E_{j\ell} R}{\hbar c(n + s + 1)}, \quad E_{j\ell} = \frac{mc^2 s}{|k|}, \quad (2.24)$$

$$\tilde{G}_{n'\ell'}^j(\chi)|_{s \rightarrow s+1} = R^{-\beta_{n'}} \sin^{-\beta_{n'}} \chi e^{-\frac{\alpha_{n'} \chi}{2}} R_{n'}^{(\alpha_{n'}, \beta_{n'})}(\cot \chi)|_{s \rightarrow s+1}, \quad (2.25)$$

$$\beta_{n'}|_{s \rightarrow s+1} = \beta_n, \quad \alpha_{n'}|_{s \rightarrow s+1} = \alpha_n, \quad n' = n - 1, \quad (2.26)$$

where  $R_n^{(\alpha_n, \beta_n)}(\cot \chi)$  are the Romanovski polynomials [26]. These polynomials can be obtained with the aid of the Rodrigues formula

$$R_n^{(\alpha_n, \beta_n)}(x) = \frac{1}{\omega^{(\alpha_n, \beta_n)}(x)} \frac{d^n}{dx^n} \left[ \omega^{(\alpha_n, \beta_n)}(x) (1 + x^2)^n \right], \quad x = \cot \chi, \quad (2.27)$$

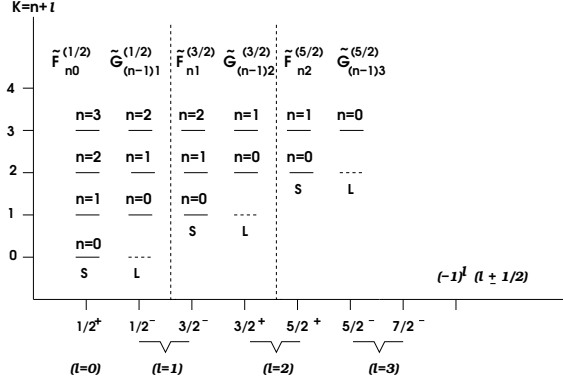


FIG. 1: Schematic presentation of the solutions  $\tilde{G}_{n'l}^j(\chi)$  and  $\tilde{F}_{n'l}^j(\chi)$  to the eqs. (2.19) and (2.20), acting as the respective upper/large (L) and lower/small (S) components of the intermediate auxiliary spinor  $\tilde{\Psi}_{j\ell}(\chi)$  in (2.13) within the SUSY-QM scheme. On the figure we separated the spinors of different  $j$  by vertical dashed lines. To be specific, the first, second, third and etc. columns illustrate the respective  $\tilde{\Psi}_{(1/2),0}(\chi)$ ,  $\tilde{\Psi}_{(3/2),1}(\chi)$ ,  $\tilde{\Psi}_{(5/2),2}(\chi)$ , and etc. spinors with rising  $n$ . The nomenclature used in the  $\tilde{\Psi}_{j\ell}(\chi)$  labeling is such that the index  $\ell$  belongs to the angular momentum underlying the lower component. The states of the highest spin possible for a given  $K$  correspond to  $n = 0$ , their  $\ell$  takes the maximal  $\ell_{\max} = K$  value, and their spins are  $j = (K + \frac{1}{2})$ . Their spinors have all only lower components. The upper components to  $n = 0$  are absent (denoted by horizontal dashed segments) because they would require according to (2.29) a node number lower by one unit than  $n$ , i.e. a prohibited negative value. These spinors describe the states of the lowest energies (ground states) in a column. In consequence, the genuine Dirac ground state spinors,  $\Psi_{j\ell}(R, \chi)$ , in (2.3) (upon accounting for (2.13)), have upper and lower components of equal functional forms, distinct by a constant. The above lying spinors are associated with solutions to the Dirac equation corresponding to energies higher than the ground state value, and their upper and lower components are of different functional forms.

and from the following weight function

$$\omega^{(\alpha_n, \beta_n)}(x) = (1 + x^2)^{\beta_n} e^{-\alpha_n \cot^{-1} x}. \quad (2.28)$$

In this fashion, the general (unnormalized) “quasi-radial” Dirac spinor in (2.3) take the form,

$$\begin{aligned} \Psi_{j\ell}(R, \chi) &= \frac{1}{2s(s+k)} \begin{pmatrix} (k+s) & \gamma \\ \gamma & (k+s) \end{pmatrix} \begin{pmatrix} \tilde{G}_{n'\ell'=(\ell+1)}^j(\chi)|_{s \rightarrow s+1} \\ \frac{R \sin \chi}{\tilde{F}_{n\ell}^j(\chi)} \\ \frac{\tilde{F}_{n\ell}^j(\chi)}{R \sin \chi} \end{pmatrix} \\ &= \frac{1}{2s(s+k)} \begin{pmatrix} (k+s) & \gamma \\ \gamma & (k+s) \end{pmatrix} \frac{R^{n+s+1} \sin^{n+s+1} \chi}{R \sin \chi} \begin{pmatrix} e^{-\frac{\gamma E_{j\ell} R \chi}{\hbar c(n+s+1)} R_{n-1}^{(\alpha_n, \beta_n)}(\cot \chi)} \\ e^{-\frac{\gamma E_{j\ell} R \chi}{\hbar c(n+s+1)} R_n^{(\alpha_n, \beta_n)}(\cot \chi)} \end{pmatrix}. \end{aligned} \quad (2.29)$$

These are the Dirac spinors which provide the basis for the relativistic description of the nucleon and its excitations.

### B. The “quasi-radial” Dirac spinor for the ground state of the proton

We here are primarily interested in the ground state for which  $\ell = n = 0$ ,  $j = 1/2$ , and  $k = -1$ , in which case the equations (2.10)-(2.11) are,

$$\left[ \frac{\hbar c}{R} \frac{d}{d\chi} + W(\chi) \right] \tilde{G}_{n'1}^{(1/2)}(\chi) = \left( mc^2 - \frac{1}{s+1} E_{(1/2)0} \right) \tilde{F}_{00}^{(1/2)}(\chi), \quad (2.30)$$

$$\left[ -\frac{\hbar c}{R} \frac{d}{d\chi} + W(\chi) \right] \tilde{F}_{00}^{(1/2)}(\chi) = \left( -\frac{1}{s+1} E_{(1/2)0} - mc^2 \right) \tilde{G}_{n'1}^{(1/2)}(\chi). \quad (2.31)$$

As explained in the caption of Fig. 1, in SUSY-QM the ground state spinor corresponds to  $n = 0$ , and is obtained upon nullifying the right hand sides of the equations (2.10), (2.11). This means that for odd  $(-1)^{j+\ell+\frac{1}{2}} = (-1)$

phases, only  $\tilde{F}_{0\ell}^j(\chi)$  can be different from zero, while  $\tilde{G}_{n'\ell'}^j(\chi)$  has to identically vanish, due to the prohibited  $n' = -1$  value. Indeed, because the coefficient  $(mc^2 - E_{(1/2)0}/(s+1))$  on the rhs in (2.30) can be zero, fixing the  $E_{(1/2)0}$  value to  $E_{(1/2)0} = mc^2/(s+1)$ , this equation can have solutions for  $\tilde{F}_{00}^{(1/2)}(\chi) \neq 0$ . On the other side, because the coefficient  $(-E_{(1/2)0}/(s+1) - mc^2)$  on the rhs in (2.31) is always different from zero, the condition defining  $\tilde{F}_{00}^{(1/2)}(\chi)$  as a ground state

$$\left[ -\frac{\hbar c}{R} \frac{d}{d\chi} + W(\chi) \right] \tilde{F}_{00}^{(1/2)}(\chi) = 0, \quad (2.32)$$

can be fulfilled only if  $\tilde{G}_{n'1}^{(1/2)}(\chi)$  in (2.31) identically vanishes

$$\tilde{G}_{n'1}^{(1/2)}(\chi) = 0, \quad \text{for } E_{(1/2)0} = \frac{s+1}{|k|} mc^2, \quad |k| = |-1| = 1, \quad s = \sqrt{1 - \alpha_s^2 N_c^2} < 1. \quad (2.33)$$

In this fashion, the Dirac spinor in (2.3) corresponding to the ground state (gst) is calculated from (2.13) and (2.9) as

$$\Psi_{(1/2)0}^{\text{gst}}(R, \chi) = N_{(1/2)0} \begin{pmatrix} \frac{iG_{(1/2)0}(\chi)}{R \sin \chi} \\ \frac{F_{(1/2)0}(\chi)}{R \sin \chi} \end{pmatrix} = N_{(1/2)0} \frac{1}{2s(s+k)} \begin{pmatrix} \frac{i\gamma \tilde{F}_{00}^{(1/2)}(\chi)}{R \sin \chi} \\ \frac{(k+s)\tilde{F}_{00}^{(1/2)}(\chi)}{R \sin \chi} \end{pmatrix}, \quad (2.34)$$

where  $N_{(1/2)0}$  is a normalization constant, while  $\tilde{F}_{00}^{(1/2)}(\chi)$  is given by

$$\tilde{F}_{00}^{(1/2)}(\chi) = R^{-\beta_0} \sin^{-\beta_0} \chi e^{-\frac{\alpha_0}{2}\chi}, \quad \alpha_0 = \frac{2\gamma mc^2 R}{|k|\hbar c}, \quad -\beta_0 = s+1, \quad (2.35)$$

where use of the equation (2.24), and (2.33) has been made. Substituting (2.35) into (2.34) shows that the choice of  $\lambda = -1$  ensured that the spinor's pre-factor  $\sin^{-\beta_0} / \sin \chi$  is finite for  $s < 1$ , and that the spinor basis obtained in this way is free from singularities.

### C. Comparison of the ‘‘quasi-radial’’ Dirac spinors to the two-component wave functions in the Light-Front Holographic QCD

The system of equations (2.19)-(2.22) resembles in certain sense, to be specified below, a similar one emerging within the Light Front Holographic QCD (LF-HQCD) [13], [14]. The latter formalism has been derived within a flat Minkowski 3+1 space time and the corresponding equations reduce to one-dimensional equations in the light front radial variable  $\zeta$  after projection on states of fixed  $J_z$  and  $L_z$ . This method has been concluded from the AdS<sub>5</sub>/CFT<sub>4</sub> gauge-gravity duality and is of a field-theoretical nature. There, one encounters the following two coupled stationary Schrödinger equations,

$$H^\nu(\zeta) \Psi_+^{n\nu}(\zeta) = \left( -\frac{d^2}{d\zeta^2} + \frac{\nu^2 - \frac{1}{4}}{\zeta^2} + \kappa^4 \zeta^2 + c_+^\nu \right) \Psi_+^{n\nu}(\zeta) = M^2 \Psi_+^{n\nu}(\zeta),$$

$$c_+^\nu = 2\kappa^2(\nu+1), \quad (2.36)$$

$$H^{\nu+1}(\zeta) \Psi_-^{n(\nu+1)}(\zeta) = \left( -\frac{d^2}{d\zeta^2} + \frac{(\nu+1)^2 - \frac{1}{4}}{\zeta^2} + \kappa^4 \zeta^2 + c_-^\nu \right) \Psi_-^{n(\nu+1)}(\zeta) = M^2 \Psi_-^{n(\nu+1)}(\zeta),$$

$$c_-^\nu = \kappa^2 \nu. \quad (2.37)$$

The solutions in (2.36)- (2.37) correspond physically to a quark with spin parallel vs. anti-parallel to the proton's helicity in the nucleon quark-diquark bound state and allow to compute the Pauli form factor from the overlap of the  $\Psi_\pm$  solutions, in which case the weights of  $\Psi_\pm$  solutions are equal.

The LF-HQCD wave functions provide a variety of dynamical predictions, among them hadron spectra, distribution amplitudes, and hadron form factors. The latter are calculated as first-principle hadronic matrix elements of the electromagnetic current and, in being derived using the Drell-Yan West formalism, are frame-independent. Also quark counting rules at high momentum transfer are satisfied.



From a purely algebraic point of view, and leaving aside the discussion on the different conceptual backgrounds of the two methods,  $AdS_5/CFT_4$  gauge-gravity duality of the latter, versus  $dS_4$  special relativity with a Dirac equation on  $S^3$  of the present [9], the LF-HQCD equations relate to our equations (2.11)-(2.12) (and vice versa) via the following replacement of the super-potential  $W(\chi)$  in (2.12),

$$\left[ W(\chi) = -\frac{\hbar c}{R} s \cot \lambda \chi - \frac{\gamma}{s} E_{j\ell} \right] \longleftrightarrow \left[ W^{LF}(\zeta) = -\frac{\nu + \frac{1}{2}}{\zeta} + \kappa^2 \zeta \right], \quad (2.38)$$

where  $\kappa^2$  is an external inverse length scale. Similarly as the super-potential in (2.12) generated our conformal partner interactions  $V_1(\chi)$  and  $V_2(\chi)$  in (2.21) and (2.22), also the super-potential  $W^{LF}(\zeta)$  in (2.38) generates in light front coordinates a pair of conformal confining interactions though of an infinite range, and composed by inverse distance square plus harmonic oscillator terms, and given by

$$V_2^{LF}(\zeta) = 4\kappa^4 \zeta^2 + \frac{\nu^2 - \frac{1}{4}}{\zeta^2} - c_+^\nu, \quad \zeta \in [0, \infty), \quad (2.39)$$

$$V_1^{LF}(\zeta) = 4\kappa^4 \zeta^2 + \frac{(\nu + 1)^2 - \frac{1}{4}}{\zeta^2} - c_-^\nu, \quad (2.40)$$

with  $c_+^\nu = 2\kappa^2(\nu + 1)$ , and  $c_-^\nu = 2\kappa^2\nu$ . The  $V_1^{LF}(\zeta)$  and  $V_2^{LF}(\zeta)$  mass spectra emerge in turn as  $M_{n\nu}^2 = 4\kappa^2 n$  and  $M_{n'\nu'}^2 = 4\kappa^2(n' + 1)$  meaning that for  $n' = n - 1$  one finds isospectrality. Obviously, for  $n = 0$ , and  $\nu' = \nu + 1$  the vacuum, same as in our case above, remains unpaired. The respective solutions,  $|n, \nu\rangle$  and  $|n' = n - 1, \nu' = \nu + 1\rangle$ , act as the counterparts to ours  $\tilde{F}_{na}^{j\ell}(\chi)$  and  $\tilde{G}_{n'a'}^{j\ell}(\chi)$  from (2.24)-(2.26). Yet, the equidistance of the harmonic oscillator excitations, absent in our case, allows for a global shift downwards by a constant of all the  $M_{n'\nu'}^2$  masses, and thereby allows to place the  $|n = 0, \nu' = \nu + 1\rangle$  partner to  $|n = 1, \nu >$  at the same mass as the originally unpaired  $|n = 0, \nu\rangle$  ground state. In this way, super-symmetric partners of equal node numbers to all the states have been created in [14], after which the Light Front spinors acquire their final shapes according to,

$$\Psi^{LF}(\zeta) = \begin{pmatrix} (\kappa^2 \zeta^2)^{\frac{\nu}{2} + \frac{1}{4}} e^{-\frac{\kappa^2 \zeta^2}{2}} L_n^\nu(\kappa^2 \zeta^2) \\ (\kappa^2 \zeta^2)^{\frac{\nu+1}{2} + \frac{1}{4}} e^{-\frac{\kappa^2 \zeta^2}{2}} L_{n+1}^{\nu+1}(\kappa^2 \zeta^2) \end{pmatrix}, \quad (2.41)$$

where  $L_n^\nu$  stand for Laguerre's polynomials. The above algebraic manipulation obliterates to some extent the parallelism between the latter equation and our (2.29), where the node numbers in the upper and lower components are distinct by one unit, as is inevitably the case for all SUSY-QM potentials except the Harmonic Oscillator.

In the following section we test the ‘‘quasi-radial’’ spinor in (2.34)-(2.35) in the calculation of the electric-charge and magnetic-dipole form factors of the proton.

### III. THE PROTON ELECTRIC-CHARGE AND MAGNETIC-DIPOLE FORM FACTORS

Form factors provide valuable insights into the internal structure of the nucleon. In particular, the electric-charge  $G_E^p(Q^2)$ , and magnetic-dipole,  $G_M^p(Q^2)$ , form factors of the proton, the subject of the current section, codify to some extent the internal electric-charge-, and magnetization-current distributions of this particle. This is so because in the Breit-frame, defined at zero energy transfer,  $\mathbf{p} = -\mathbf{p}'$ , they can be defined [27] as the Fourier transforms the corresponding electric-charge-, and magnetization-current densities in position space,  $\rho^p(r)$ , and  $\rho_{\text{mgn}}^p(r)$ ,

$$G_E^p(Q^2) = \int_0^\infty \rho^p(r) e^{i\mathbf{r}\cdot\mathbf{q}} d\mathbf{r}, \quad (3.1)$$

$$G_M^p(Q^2) = \int_0^\infty \rho_{\text{mgn}}^p(r) e^{i\mathbf{r}\cdot\mathbf{q}} d\mathbf{r}. \quad (3.2)$$

where the transferred four-momentum is space-like,  $-q^2 = Q^2 \geq 0$ . In terms of Dirac spinors and their components, one finds

$$\rho^p(r) = |\Psi_{j\ell}(r)|^2 = G_{(1/2)0}^2(r) + F_{(1/2)0}^2(r), \quad (3.3)$$

$$\rho_{\text{mgn}}^p(r) = \bar{\Psi}_{j\ell}(r) \gamma_5 \Psi_{j\ell}(r) = \frac{2G_{(1/2)0}(r)F_{(1/2)0}(r)}{Q} \mu_N \frac{\partial}{\partial r}, \quad (3.4)$$

where  $\mu_N$  stands for Bohr's nuclear magneton,  $\mu_N = \frac{\hbar c}{M_p c^2}$ . In effect, the form factors  $G_E^p(Q^2)$  and  $G_M^p(Q^2)$  can be expressed as the following integrals [28]-[29],

$$G_E^p(Q^2) = \int_0^\infty \left( G_{(1/2)0}^2(r) + F_{(1/2)0}^2(r) \right) j_0(Qr) dr, \quad (3.5)$$

$$G_M^p(Q^2) = \int_0^\infty \frac{2G_{(1/2)0}(r)F_{(1/2)0}(r)}{Q} \mu_N j_1(Qr) dr. \quad (3.6)$$

At zero momentum transfer, these form factors are normalized as  $G_E^p(0) = e_p = 1$ , where  $e_p$  is the proton electric charge, and  $G_M^p(0) = \mu_p$ , with  $\mu_p$  standing for the magnetic dipole moment, whose experimental value is reported as  $\mu_p = 2.79284734462(82)\mu_N$  in [2].

The goal of the present section is to test as to what extent the ground state Dirac spinor in (2.34) with the function in (2.35) is capable of capturing the essentials of the internal proton electromagnetic structure. In order to account for the property of the wave function to be defined over a finite interval, the Fourier transform has to be properly modified. Integral transforms of functions defined on finite intervals on the real line have been studied for example in [30], where the modification of the plane wave has been obtained as

$$e^{iqr \cos \theta} \longrightarrow e^{iqR\chi \cos \theta}, \quad \chi \in [0, \pi], \quad (3.7)$$

amounting with the aid of (2.34), (2.35) to

$$G_E^p(Q^2) = N_1 \int_0^\pi |\tilde{F}_{00}^{(1/2)}(\chi)|^2 j_0(QR\chi) dR\chi, \quad (3.8)$$

$$\frac{G_M^p(Q^2)}{\mu_N} = N_2 \int_0^\pi |\tilde{F}_{00}^{(1/2)}(\chi)|^2 \frac{j_1(QR\chi)}{Q} dR\chi, \quad (3.9)$$

where  $N_1$  and  $N_2$  are constants related to the spinor normalization accounting for (2.13).

In so doing, the explicit expressions for the integrals to be evaluated below become

$$G_E^p(Q^2) = N_1 \int_0^\pi \sin^{2(s+1)} \chi \exp(-\alpha_0 \chi) j_0(RQ\chi) dR\chi, \quad (3.10)$$

$$\frac{G_M^p(Q^2)}{\mu_N} = N_2 \int_0^\pi \sin^{2(s+1)} \chi \exp(-\alpha_0 \chi) \frac{j_1(RQ\chi)}{RQ} dR\chi, \quad (3.11)$$

$$s = \sqrt{1 - \alpha_s^2 N_c^2}, \quad \alpha_0 = 2\sqrt{1 - \alpha_s^2 N_c^2} \frac{mc^2 R}{\hbar c}. \quad (3.12)$$

In the following we seek for values of the three parameters:  $s$  (related to  $\beta_0$  in (2.35)),  $R$ , and  $\alpha_0$  for which the experimental data on  $G_E^p(Q^2)$ , and  $G_M^p(Q^2)$ , together with their ratio, all taken from [31] can be adjusted by the expressions in (3.10), and (3.11), respectively.

For that purpose we run a least mean square fit procedure over the entire data set including  $G_E^p(Q^2)$ ,  $G_M^p(Q^2)/\mu_p$ , and  $\mu_p G_E^p(Q^2)/G_M^p(Q^2)$ , finding the following parameter values:

$$\beta_0 = -1.143789, \quad \frac{\alpha_0}{2} = 2.60695, \quad R = 1.10773 \text{ fm}. \quad (3.13)$$

The ratios of the form-factors under investigation to the dipole function  $G_D = \left(1 + \frac{Q^2}{0.71}\right)^{-2}$  are plotted and compared to data in Fig. 2, while the  $\mu_p G_E^p/Q^2$  ratio is displayed in Fig. 3. The figures convincingly show that the calculations realistically capture the proton's spin physics and the measured shapes of the two form factors under consideration. Our results compare in quality to the predictions of the light-front holographic formalism [32] as well as other adequate models reviewed in [33].

It has to be stressed that the exponential fall-off of the Dirac spinor wave function, brought about by the color confining dipole potential in (2.4) that effectively accounts for confinement, has been crucial for the satisfactory data description. For this reason we conclude that the potential in (2.4) adequately accounts for the perception of color confinement by the proton's electromagnetic form-factors.

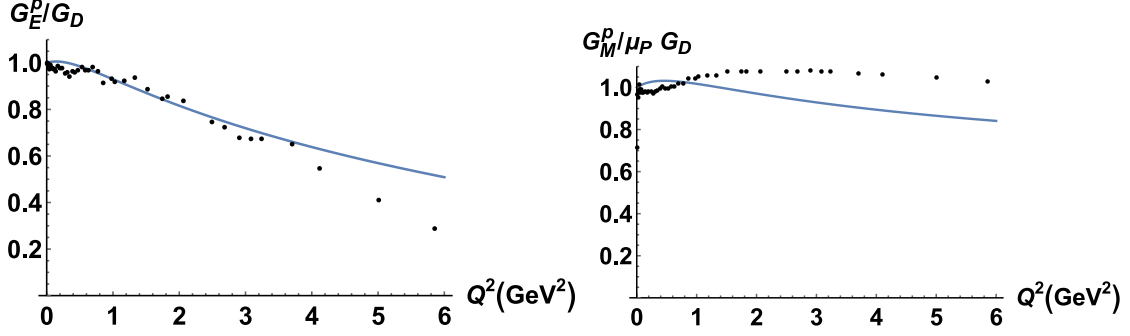


FIG. 2: The ratios of the proton's electric charge  $G_E^p$ , and magnetic-dipole,  $G_M^p/\mu_p$ , form-factors with the dipole function,  $G_D = \left(1 + \frac{Q^2}{0.71}\right)^{-2}$ , each normalized to one at origin, and calculated with the best fit parameter set in (3.13). Data taken from [31] and marked by points.

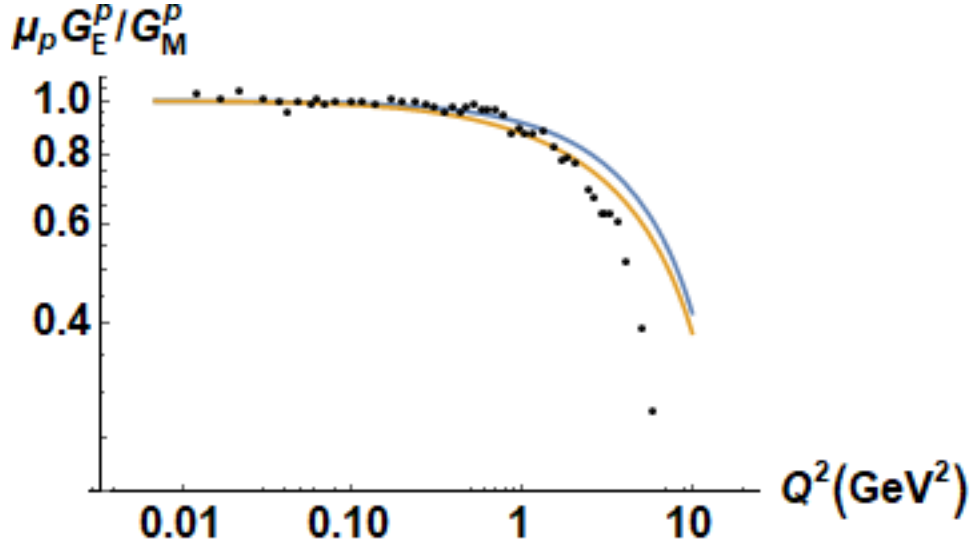


FIG. 3: The  $\mu_p G_E^p / G_M^p$  ratio for the numerically evaluated form factors displayed in the Figures 2 (yellow line) and for the analytic expressions in (3.14) and (3.15) (blue line) on a logarithmic  $Q^2$  scale of the horizontal axis. Data taken from [31] and marked by points.

We furthermore observe that as visualized by Fig. 4, the probability densities calculated once with the exact function  $\tilde{F}_{00}^{(1/2)}(\chi)$  in (2.35), and then by its approximated form corresponding to,  $R \sin^{s+1} \chi \approx R \chi^{s+1}$ , are practically coincident for the set of parameters in (3.13). Thanks to this circumstance, our “quasi-radial” Dirac equation effectively behaves as a flat-space radial equation though with a potential defined on a finite interval of the real line, a circumstance that in the hindsight justifies usage of the standard formulas in [27].

Moreover, extending in this very approximation the integration in (3.10)-(3.11) towards the mathematically permitted infinity, practically does not alter the numerical results, but brings the advantage to allow one to express the corresponding integrals, each normalized to one at origin, in closed form, which we obtained by the symbolic software Mathematica as,

$$G_E^p(Q^2) = \frac{1}{(1+y^2)^{1+s}} \frac{\sin(2(1+s)\tan^{-1}y)}{2(1+s)y}, \quad y = \frac{QR}{\hbar c \alpha_0}, \quad (3.14)$$

and

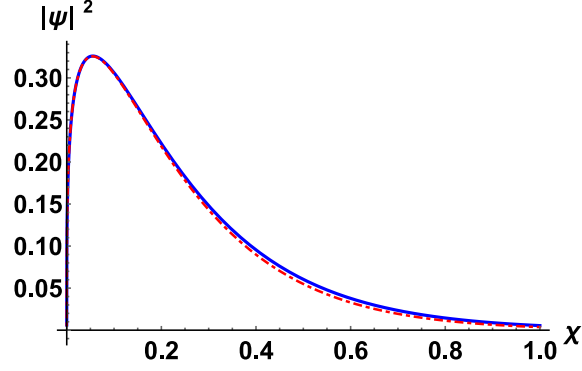


FIG. 4: The shape of the probability density in the ground state,  $|\Psi_{1/2,0}^{(\text{gst})}(\chi)|^2$ , denoted in the figure by  $|\Psi|^2$ , and calculated for the parameters in (3.13) once with the exact wave function from eqs. (2.34)-(2.35) (solid line), and then in the  $\sin \chi \approx \chi$  approximation (dashed line).

$$\begin{aligned} \frac{G_M^p(Q^2)}{\mu_p} &= \frac{1}{(1+y^2)^{1+s}} \frac{3}{2(1+s)(3+2s)y^2} \\ &\times \left( \frac{(1+y^2)^{\frac{1}{2}}}{(1+2s)y} \sin((1+2s)\tan^{-1}y) - \cos(2(1+s)\tan^{-1}y) \right). \end{aligned} \quad (3.15)$$

The comparison of the above expressions to the numerical results is shown in Fig. 3. Finally, we also calculated the proton's charge and magnetic root mean-square radius and magnetic moment [34], finding the following values,

$$\sqrt{\langle r_p^2 \rangle_E} = \sqrt{\langle (R\chi)^2 \rangle} = \sqrt{\frac{R^2(4+2s)(3+2s)}{\alpha_0^2}} = 0.79765 \text{ fm}, \quad (3.16)$$

$$\sqrt{\langle r_p^2 \rangle_M} = \sqrt{\frac{12R^2(2+s)(5+2s)}{10\alpha_0^2}} = 0.78358 \text{ fm}, \quad (3.17)$$

$$\begin{aligned} \frac{\mu_p}{\mu_N} &= \frac{2}{3} \frac{M_p c^2}{\hbar c} \gamma \langle R\chi \rangle \\ &= \frac{2}{3} \frac{M_p c^2 \gamma R}{\hbar c} \frac{\Gamma(4+2s)}{2\alpha_0(1+s)\Gamma(2+2s)} = \frac{2}{3} \frac{M_p c^2 \gamma R}{\hbar c} \frac{(3+2s)}{\alpha_0} = 2.1910. \end{aligned} \quad (3.18)$$

The proton charge root mean square radius lies by about 9 % below the data point of 0.84184(67) reported in [35], while  $\mu_p$  underestimates the well known experimental value [2] of 2.79284734462(82) $\mu_N$  by about 20%. We explain the latter circumstance by the fact that we extracted the model parameters by fitting the  $G_E^p$  and  $G_M^p/\mu_p$  data and then calculated  $\mu_p$  with these parameters according to the expression given in (3.18). Stated differently, the  $\mu_p$  value has not been explicitly included as an observable to be adjusted by the fit. Our predicted proton magnetic radius underestimates the data point of  $0.86_{-0.03}^{+0.02}$  reported in [36] by about 9%. Nonetheless, in our opinion the results obtained are all pretty reasonable especially in view of the fact that they all have been evaluated by employing same set of three parameters in (3.13). The parameters  $\gamma$ ,  $\alpha_0$  and  $s$  entering the expressions in (3.16)-(3.18) have been previously defined in the above equations (2.7), (2.8), and (2.35). Their numerical values correspond to (3.13).

A comment is in place on criticism regarding the frame-dependence of the Sachs form-factors [37]. Our model at the present stage is not formulated in a Lorentz covariant fashion, though this is not a conceptual problem but rather technical issue. Indeed, as explained above in (and around) the equation (1.9), the  $S^3$  Laplacian can be transformed to the effective Minkowski metric as explained around and in the equation (1.9). On such a plane Minkowski space-(conformal)time one can define Lorentz transformations, four vectors, covariant couplings to the electromagnetic field, and even switch to light-front variables, a project for future research, whose mentioning here

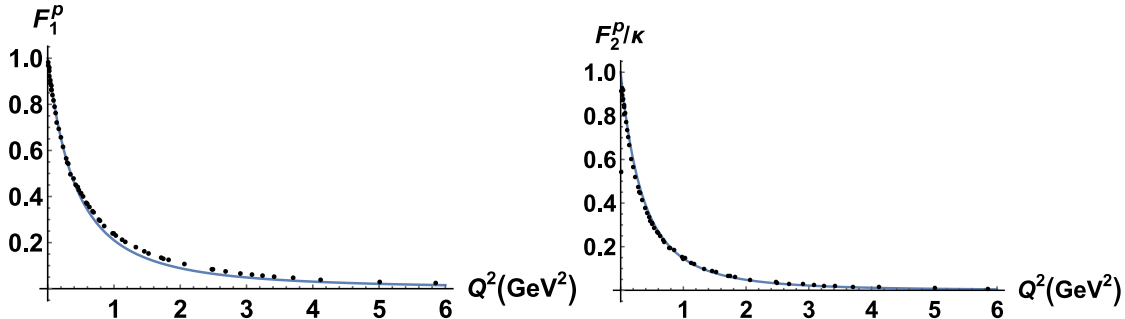


FIG. 5: Dirac's  $F_1^p$  (left) and  $F_2^p$  (right) form factors. Data taken from [32] and marked by points.

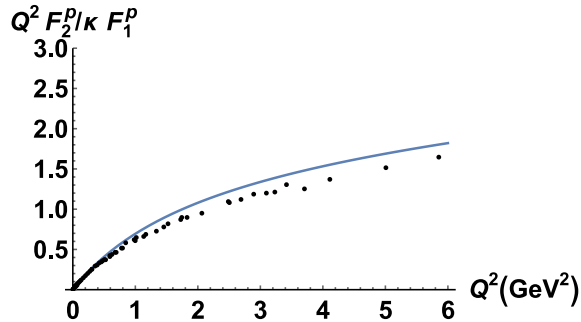


FIG. 6: The  $Q^2 F_2^p / F_1^p$  ratio. Data taken from [32] and marked by points.

has the purpose to point out that Lorentz invariance must not be beyond reach of models formulated on closed spaces. Surprisingly, the lack of manifest Lorentz covariance of the model under investigation seems to have a minor effect on its predictions. Indeed, we extracted the Dirac form factors  $F_1^p(Q^2)$  and  $F_2^p(Q^2)$  from  $G_E^p(Q^2)$  and  $G_M^p(Q^2)$  as

$$F_1^p(Q^2) = \frac{G_E^p(Q^2) + \frac{Q^2}{4M^2} G_M^p(Q^2)}{1 + \frac{Q^2}{4M^2}}, \quad (3.19)$$

$$\kappa F_2^p(Q^2) = \frac{G_M^p(Q^2) - G_E^p(Q^2)}{1 + \frac{Q^2}{4M^2}}, \quad (3.20)$$

using our calculated  $\kappa = 1.191$  value and the experimental proton mass, and compared to the data set reported in [38], also used in [32] in the evaluation of hadron electromagnetic form-factors within the LF-HQCD theory. The results are shown in Figs. 5,6. No significant discrepancy between predictions and data is observed for the Pauli form factor  $F_2$ . However one expects the Dirac form-factor,  $F_1$ , whose  $Q^2$  dependence is more complicated than that of  $F_2$ , to be more affected by Lorentz boost effects. Indeed, in  $F_1$  one observes a small but detectable underestimation of data within the region between  $0.5 \text{ GeV}^2$  to  $2 \text{ GeV}^2$  where Lorentz effects are expected to be viable. We interpret this minor deviation from data as an artifact of the missing Lorentz invariance of our method in its present form. However, at the same time, we think that the smallness of the effect and its gradual disappearance at higher  $Q^2$  is due to the favorable rôle played by the exponential fall off of the Dirac wave functions which above  $2 \text{ GeV}^2$  seem to take over Lorentz boost corrections. In conclusion, we interpret the satisfactory description of the proton electromagnetic form factors within our framework as a supremacy over the kinematic Lorentz invariance of the dynamical conformal symmetry, implemented by the Dirac equation of the present method in a way similar to the LF-HQCD Dirac equation.

As one more test of the credibility of the here advocated model we check below compatibility of our predicted  $\mu_n/\mu_p$  ratio with data. The most immediate approach to the neutron magnetic dipole moment,  $\mu_n$ , in units of  $\mu_N$ , within the present framework is found through its electric charge form factor and its relationship to the respective proton form factor while making use of a Galster inspired parametrization [39], here chosen as

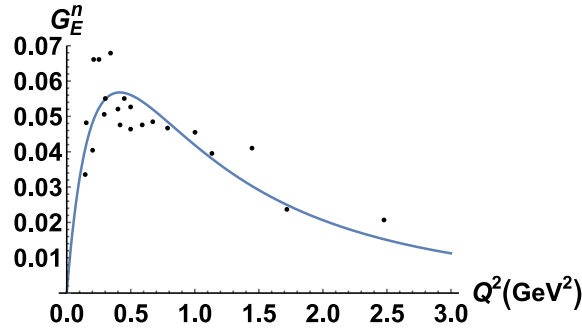


FIG. 7: The electric charge form factor of the neutron following from (3.21) (solid line) for  $B = 2.54061$  and  $\mu_n = -1.586\mu_N$  in comparison to data taken from [39] (points). The accuracy of the fit is illustrated by the value of  $\sigma_E^n = \sqrt{\sum_{i=1}^{i=N} ([G_E^n(Q_i^2)]^{th} - [G_E^n(Q_i^2)]^*)^2} / (N - N_P) = 0.00789728$ , where asterisks denotes the data points,  $N = 22$  is the number of data points, while  $N_P = 2$  refers to the number of parameters.

$$G_E^n(Q^2) = -\frac{\mu_n \tau}{1 + B\tau} G_E^p(Q^2), \quad \tau = \frac{Q^2}{4M_n^2}. \quad (3.21)$$

In adjusting by the  $\mu_n$  and  $B$  parameters the expression in (3.21) to the data taken from [39], the  $\mu_n$ -value emerges as

$$\mu_n = -1.58661\mu_N, \quad (3.22)$$

and similarly to the proton's magnetic dipole moment, underestimates the data point given by,  $-1.91304245(45)\mu_N$ , by about 20%. The resulting  $\mu_n/\mu_P$  ratio,

$$\frac{\mu_n}{\mu_p} = -0.7244, \quad (3.23)$$

overestimates the experimental data point of,  $-0.68497934(16)$ , by only few percents. The neutron's electric charge form-factor is displayed in Fig. 7.

Finally, our approach also allows for a convenient parametrization of the neutron magnetic form factor,  $G_M^n(Q^2)$  in so far as when normalized to one at origin,  $G_M^n(Q^2)/\mu_n$ , it can be pretty well approximated by the normalized proton magnetic form factor,  $G_M^p(Q^2)/\mu_p$ . In this way, equality of the proton and neutron magnetic radii is predicted. Such an approximation is compatible with the fact that the neutron's magnetic radius,  $r_M^n = 0.88 \pm 0.05\text{fm}$  [36], is by about only 2% larger than the proton's magnetic radius. The comparison of  $G_M^n(Q^2) = \mu_n G_M^p(Q^2)/\mu_p$  to data is displayed in Fig. 8, and presents itself pretty convenient, indeed.

Recapitulating, the framework presented here provides a reasonable description of the proton's electric-charge and magnetic-dipole form factors together with their ratio. Also the neutron's charge and magnetic form factors came out reasonably, amounting to a  $\mu_n/\mu_p$  ratio in a good agreement with data. Furthermore, the proton's electric-charge and magnetic radii have been recovered within an accuracy of few percents. As a result, a variety of observables could be predicted within acceptable range of accuracy by the aid of only three parameters. Such has been possible, in our opinion, by the virtue of the conformal symmetry of the non-power quark potential defining the Dirac spinors of the proton.

Before closing the current section, we like to recall on the relationships of the model parameters to fundamental constants in QCD. As repeatedly stressed through the text, the magnitude of the potential used was determined by the product of the strong coupling  $\alpha_s$  and the numbers of colors,  $N_c$  in QCD. In adopting the established  $N_c = 3$  value, the partner potentials in (2.21)-(2.22) depend on the parameter  $\alpha_s$ , absorbed by  $\beta_0$  in (2.35) in combination with (2.8), and, via  $E_{j\ell}$  in (2.33), on the mass parameter  $mc^2$ , absorbed by  $\alpha_0$  in (2.35). In being less than the nucleon mass, this  $mc^2$  parameter comes out pretty reasonable. However, so far we have not elaborated any approach to the extraction of the nucleon mass from the reduced mass. Therefore, the fit by the two parameters,

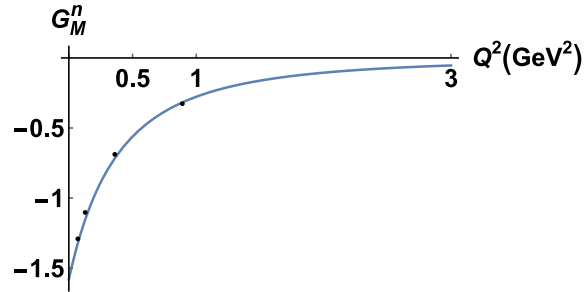


FIG. 8: The neutron magnetic form factor,  $G_M^n(Q^2)$ , here denoted by  $G_M^n$ , and calculated as  $G_M^n(Q^2) = \mu_n G_M^p(Q^2)/\mu_p$  with  $\mu_n$  and  $G_M^p(Q^2)$  from the respective eqs. (3.22), and (3.15), and with the same parameter set in (3.13). As trim points representative of the experimental data set we have chosen the four data points reported in the Table 2 of ref. [40]. There, the measurements have been performed at  $Q^2$  values of  $Q^2 = 0.071, 0.125, 0.359, \text{ and } 0.894 \text{ GeV}^2$ , and the  $G_M^n/(\mu_n G_D)$  values (with  $G_D$  as always standing for the dipole function already given in the caption to Fig. 2) have been extracted as  $0.990 \pm 0.013, 0.967 \pm 0.013, 0.989 \pm 0.014, \text{ and } 1.062 \pm 0.014$ , respectively. The figure shows that our parametrization captures well the tendency of data modulo that data extrapolate at origin at  $\mu_n = -1.91304245(45)\mu_N$  while in our calculation the absolute value of this point appears by about 20% lower the experimental one.

form factors	$\alpha_s$	$mc^2$ [MeV]	$R$ [fm]	$\sigma_{E/M}^p$
$G_E^p$	0.3298	469.27	1.10773	0.0135263
$G_M^p$	0.3298	469.27	1.10773	0.0461983

TABLE I: Values of the strong coupling,  $\alpha_s$ , and the mass  $mc^2$  parameter (first and second columns) extracted from fitting proton's electric-charge and magnetic-dipole form factors together with their ratio by the parameters  $\beta_0$  and  $\alpha_0$  in (3.13). The third column contains the values of the length scale  $R$  from same parameter set (3.13). In the last column the  $\sigma_{E/M}$

value, illustrative of the quality of our data fit, is defined as,  $\sigma_{E/M}^p = \sqrt{\sum_{i=1}^{i=N} \left( \left[ G_{E/M}^p(Q_i^2) \right]^{th} - \left[ G_{E/M}^p(Q_i^2) \right]^* \right)^2} / (N - N_p)$ , with the asterisks denoting the experimental data points whose number is  $N = 47$ , while  $N_p = 3$  stands for the number of the three recurring parameters.

$\beta_0$ , and  $\alpha_0$  in (3.13) can be converted to a fit by  $\alpha_s$ , and a mass. The Table I shows these values. We interpret the small constant value for  $\alpha_s$  as an average of the running coupling,  $\alpha_s(Q^2)$ , over the  $0 \leq Q^2 < 6 \text{ MeV}^2$  range of evaluation of the form-factors under investigation.

It is perhaps also interesting to notice that applying the present formalism to the H Atom, i.e. placing it on a closed  $S^3$  space, predicts a hyper-radius value of the order of  $10^{-3} \text{ cm}$  and thereby by eight orders of magnitude larger than the  $H$  Atom size, a result concluded from fitting magnetic dipole matrix elements to hydrogen hyper-fine structure effects [21]. In contrast, the hyper-radius of the strong space obtained here is of the order of  $10^{-13} \text{ cm}$  and comparable with the nucleon size. Stated differently, electromagnetic processes show a clear preference towards a plane space-time, where standard electrodynamics can be applied in the evaluation of the physical properties of the electron, such as its gyromagnetic factor.

#### IV. SUMMARY AND CONCLUSIONS

The goal of the present work has been to study influence of dynamical conformal symmetry and color confinement in the infrared on proton's electromagnetic form factors through employing in a Dirac equation a non-power (trigonometric) potential with these properties, which has earlier been shown in [9],[10] to be suited for description of meson spectra. The potential is given in the above eq. (2.4), and allowed one to obtain spinor-wave functions adequate for the evaluation of the observables under investigation. The Dirac equation with this interaction has been formulated and approximately solved by the tools of the super-symmetric quantum mechanics. The solutions have then been employed in the evaluation of the electric-charge and magnetic-dipole form factors of the proton, their ratio, the electric-charge and magnetic-dipole form factors of the neutron, the root mean square charge and magnetic proton radii, the proton and neutron magnetic moments and their ratio, finding not only pretty good

data description by the same set of parameters in (3.13), but also quite reasonable approximations to the numerical results by the closed form expressions, given among others in (3.14)-(3.15), and (3.16)-(3.18). Our analyzes revealed the notable role played specifically by the color confinement, that ensured a satisfactory data description mainly in providing the exponential fall-off of the Dirac spinor wave function in (2.35) by virtue of the color confining and conformal dipole potential in (2.4). We conclude that dynamical conformal symmetry and color confinement in the infrared are compatible with data on the electric-charge and the magnetic-dipole form factors of the proton, as well as with the deviation of their ratio from the dipole scaling rule. We hope that the present study could convincingly demonstrate utility of non-power potentials in quark models.

- 
- [1] Fayyazuddin, Riazuddin, *A Modern Introduction to Particle Physics*, 2nd edition, (World Scientific, Singapore, 2000)
- [2] K. A. Olive *et al.* ( Particle Data Group), Review of Particle Physics, Chinese Physics C **38**, 090001 (2014) and 2015 update.
- [3] A. Deur, V. Burkert, J. P. Chen, W. Korsch, Phys. Lett. **665**, 349 (2008).
- [4] S. S. Afonin, Eur.Phys.J. A **29**, 327 (2006).
- [5] P. Gonzalez, Phys. Rev. D **80**, 054010 (2009).
- [6] S. S. Afonin, Mod. Phys. Lett. A **32**, 1750155 (2017).
- [7] F. Cooper, A. Khare, U. P. Sukhatme, *Supersymmetry in Quantum Mechanics* (World Scientific, Singapore, 2001).
- [8] S. Fubini, A. J. Hanson, and R. Jackiw, Phys. Rev. D **7**, 1732 (1972).
- [9] M. Kirchbach, C. B. Compean, Eur.Phys.J. A **52**, 210 (2016).
- [10] M. Kirchbach, C. B. Compean, Eur.Phys. J. A **53**, 65 (2017).
- [11] A. V. Belitsky, A. S. Gorsky, G. P. Korchemsky, Nucl. Phys. B **67**, 3 (2003).
- [12] A. Gorsky, Theor. Math. Phys. **142**, 153 (2005).
- [13] S. J. Brodsky, G. de T eramond, M. Karliner, Ann. Rev. Nucl. Part. Sci. **62**, 1 (2012).
- [14] S. J. Brodsky, Guy F. de T eramond, H.-G. Dosch, Phys. Lett. **B 729**, 3 (2014).
- [15] L. D. Landau and E. M. Lifschitz, *The Classical Theory of Fields*, Vol. 2 of A Course of Theoretical Physics, 3d edition (Pergamon Press 1971) p.335.
- [16] R. Aldrovandi, J. P. Beltr an Almeida, J. G. Pereira, Class. Quant. Grav. **24**, 1385 (2007).
- [17] M. G ockeler, T. Sch ucker, *Differential geometry, gauge theories, and gravity* (Cambridge Monographs on Mathematical Physics, Cambridge University Press, Cambridge, 1987).
- [18] M. Serna, K. Cahill, JHEP 0310, 054 (2003).
- [19] M. Bauer, D. Z. Freedman, P. E. Haagensen, Nucl. Phys. **428**, 147 (1994).
- [20] N. Bessis, G. Bessis, R. Shamseddine, Phys. Rev. A **29**, 2735-2388 (1984).
- [21] N. Bessis, G. Bessis, and R. Shamseddine, J. Phys. A:Math.Ge., **15**, 3131 (1982).
- [22] E. M. Ovsyuk, Non-linear Phenomena in Complex Systems, **14**, 1 (2011).
- [23] C. V. Sukumar, J. Phys. A:Math.Gen. **18**, L697 (1985).
- [24] K. Faegri Jr., K. G. Dylla, in *Relativistic Electron Structure Theory-Fundamentals, Part 1.*, ed. P. Schwerdtfegen (Elsevier, Amsterdam, 2003) pp. 259-288.
- [25] C. B. Compean, M. Kirchbach, J. Phys. A:Math.Gen. **39**, 347 (2006).
- [26] A. P. Raposo, H.-J. Weber, D. E. Alvarez Castillo, and M. Kirchbach, Centr. Eur. J. Phys. **5**, 253 (2007).
- [27] J. Kelley, *Nucleon charge and magnetization densities from Sachs form factors*, E-Print arXiv:hep-ph/0204239
- [28] D. H. Lu, A. W. Thomas, A. G. Williams, Phys. Rev. C **57**, 2628 (1998).
- [29] D. H. Lu, Sh. Nan Yang, A. W. Thomas, J. Phys. G:Nucl.Part.Phys. **6**, L75 (2000).
- [30] M. A. Alonso, G. S. Pogosyan, K. B. Wolf, J. Math. Phys. **44**, 1472 (2003).
- [31] J. Arrington, Phys. Rev. C **76**, 035205 (2007).
- [32] Dipankar Chakrabart and Chandan Mondal, Eur.Phys.J. C **73**, 2671 (2013).
- [33] C. F. Perdrisat, V. Punjabi, M. Vanderhaeghen, Progr. Part. Nucl. Phys. **59**, 694 (2007).
- [34] P. F. Smith, J. D. Lewin, Phys. Lett. B **94**, 484 (1980).
- [35] R. Pohl *et al.*, Nature **466**, 213 (2010).
- [36] I. T. Lorenz, H.-W. Hammer, and Ulf-G. Meißner, Eur. Phys. J. A **48** 11, 151 (2012).
- [37] Gerald A. Miller, John Arrington, Phys. Rev. C **78**, 032201 (R) (2008);  
www.phy.anl.gov/theory/PHYTI/09\_fichiers/millerANL09.pdf
- [38] G. D. Cates, C. W. de Jager, S. Riordan and B. Woitsekhowsi, Phys. Rev. Lett. **106**, 252003 (2011).
- [39] T. R. Gentile, C. B. Crawford, Phys. Rev. C **83**, 055203 (2011).
- [40] G. Kubon *et al.*, Phys. Lett. B **524**, 26 (2002).